

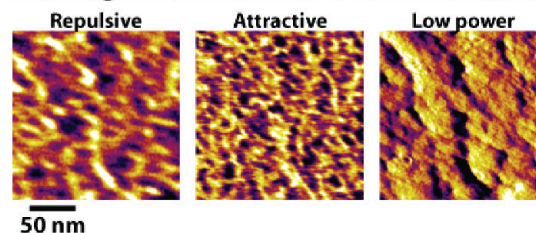
# Phase Imaging of Proton Exchange Membranes under Attractive and Repulsive Tip–Sample Interaction Forces

James R. O'Dea and Steven K. Buratto\*

Department of Chemistry and Biochemistry, University of California, Santa Barbara, Santa Barbara, California 93106-9510, United States

**S** Supporting Information

**ABSTRACT:** The nature of tip–sample interaction forces in atomic force microscopy (AFM) phase imaging strongly affects the resolution of proton conducting domains mapped at the surface of Nafion membranes. Images acquired in repulsive mode overestimated the area of individual proton conducting domains by a factor of 4 (360 vs 90 nm<sup>2</sup>) and underestimated the number of these domains by a factor of 3 (0.9 domains per 1000 nm<sup>2</sup> vs 2.7 domains per 1000 nm<sup>2</sup>) compared to attractive mode. When the cantilever was driven above resonance or when the combination of scan parameters resulted in an AFM feedback loop that was not fully optimized, phase contrast arose not from proton conducting domains but instead from changes in topography. In attractive mode, phase contrast did not correlate with either topography or changes in topography, and the resulting images most accurately represent the fluorocarbon and aqueous domains at the surface of Nafion membranes.

**Phase images of the same area of a Nafion membrane****INTRODUCTION**

Limitations in materials currently used as proton exchange membranes (PEMs) necessitate the development of next-generation, higher performing membranes.<sup>1</sup> Knowing the distribution and morphology of aqueous domains in PEMs facilitates an understanding of properties related to fuel cell performance. The ability to rationalize properties such as proton conductivity and water sorption enables feedback between such properties and molecular design of novel PEMs.<sup>2</sup> Atomic force microscopy (AFM) phase imaging has emerged as a cornerstone technique to investigate the nanoscale morphology of PEMs.<sup>3–11</sup> The ability to acquire AFM images at varied temperatures and relative humidities and to probe PEMs without alteration from the form used in fuel cells makes AFM well suited for describing the nanoscale properties of PEMs at conditions relevant to fuel cell operation. As opposed to bulk analysis techniques such as small-angle X-ray scattering,<sup>12</sup> AFM probes individual domains at the surface of a PEM. While the surface of a material does not necessarily reflect the bulk, proton conduction in PEMs is ultimately manifested at the surface of a membrane. Coupled with emerging nanoscale conductivity measurements of PEMs,<sup>8,11,13–16</sup> phase imaging can reveal the fraction of hydrophilic surface domains that are electrochemically active and contribute to the performance of a fuel cell.<sup>7</sup> phase imaging can also be used with lithography techniques to quantify the top to bottom connectivity of proton conducting domains.<sup>6</sup> Taken with internal views gained by depositing metals in the aqueous domains of PEMs,<sup>17,18</sup> surface techniques such as phase imaging enable a complete description of proton conducting domains. In this paper we show that phase imaging can be used to map the

aqueous domains at the surface of Nafion membranes, but the spatial resolution and interpretation of such domains depends strongly on the nature of tip–sample interactions.

Phase images are acquired in AC mode AFM in which a cantilever with a sharp, protruding tip is sinusoidally driven at or near its resonance frequency as it is scanned across the sample. In AC mode, the probe's oscillation amplitude is used as feedback such that the cantilever is raised or lowered in order to maintain an amplitude set point. Oscillating the cantilever while scanning not only reduces tip induced sample damage, an important consideration when studying polymers such as PEMs, but also enables mapping of the cantilever's phase relative to its drive frequency. For a sinusoidal response of an oscillating cantilever interacting with a surface, positive phase shifts (temporal leads) or negative phase shifts (temporal lags) are often expressed in degrees ( $\phi$ ) and are related to the power dissipated by tip–sample interactions ( $P_{\text{tip-sample}}$ ):<sup>19,20</sup>

$$P_{\text{tip-sample}} = \frac{1}{2} \frac{kA^2\omega}{Q} \left[ \left( \frac{QA_0}{A} \right) \sin \phi - \frac{\omega}{\omega_0} \right] \quad (1)$$

where  $k$  is the cantilever's spring constant,  $A$  is the amplitude of the cantilever as the tip interacts with the surface,  $A_0$  is the amplitude of the freely oscillating cantilever,  $Q$  is the probe's quality factor (cantilevers with high  $Q$  experience less power loss),  $\omega_0$  is the resonance frequency of the probe, and  $\omega$  is the drive frequency.

**Received:** September 15, 2010**Revised:** December 13, 2010**Published:** January 10, 2011

From 1, it is the sine of the phase angle that is related to power dissipation. Thus, maximum dissipation occurs at a response  $90^\circ$  out phase with the drive. It has been shown that attractive tip-sample interactions (negative net force) are responsible for phase shifts above  $90^\circ$  and repulsive interactions (positive net force) for phase shifts below  $90^\circ$ .<sup>21</sup> Through selection of AFM scan parameters, one can control whether attractive or repulsive forces dominate. Furthermore, because sine is symmetric about  $90^\circ$ , there are two values of  $\varphi$  that give equivalent power dissipations. Thus, it is possible for phase contrast to arise from jumps about  $90^\circ$ .<sup>19</sup> Image artifacts associated with such bistable imaging have clear signatures and have been illustrated for polymer systems, including PEMs.<sup>4</sup>

The relation between phase shifts and tip-sample power dissipations allows mapping of chemical domains based on expected differences in tip-sample interactions associated with different chemical groups.<sup>22</sup> In PEMs, which contain hydrophilic and hydrophobic moieties, phase contrast has been interpreted as arising from different tip-sample interactions associated with these domains.<sup>3,4</sup> Here, we describe results showing significant differences in the size and occurrence of hydrophilic domains mapped at the surface of the same PEM in attractive and repulsive modes, highlighting the importance of controlling tip-sample forces when describing proton conducting domains with AFM. We also report imaging conditions in which phase contrast in PEMs is not related to hydrophilic and hydrophobic domains but to changes in topography, which if unnoticed, would yield false assignment of surface features.

To illustrate the differences in attractive and repulsive mode images with regard to proton exchange membranes, we have chosen DuPont's Nafion membrane, the benchmark PEM, as a model system for this study. In this polymer, hydrophilic and hydrophobic domain separation is the result of a sulfonic acid containing side chain and a fluorocarbon backbone, respectively, with proton conduction facilitated by the former.<sup>23,24</sup>

## EXPERIMENTAL SECTION

Height and phase images were acquired with an atomic force microscope (Asylum Research, MFP-3D) using silicon probes (MikroMasch, NSC15,  $k \sim 40$  N/m,  $Q \sim 750$ ,  $\omega_0 \sim 330$  kHz, radius of curvature  $< 10$  nm). All images were taken at ambient conditions on DuPont's Nafion 212 membrane (Clean Fuel Cell Energy) as received in  $H^+$  form. No differences in domain coverage, size, or occurrence were observed as a function of ambient relative humidity, which was monitored daily and varied from 30% to 70% over the course of 12 months. This result is in agreement with Zawodzinski et al.,<sup>25</sup> who reported that, from  $\sim 15\%$  to 60% relative humidity, the water content of Nafion membranes only increases from 2 mol  $H_2O$ /mol  $SO_3^-$  to 4 mol  $H_2O$ /mol  $SO_3^-$ . While morphological changes may accompany this slight increase in water content, such changes were not measurable with AFM in this work. We do expect noticeable changes in Nafion's morphology at higher relative humidities as Zawodzinski et al.<sup>25</sup> report Nafion's water content increases from 6 mol  $H_2O$ /mol  $SO_3^-$  to 13 mol  $H_2O$ /mol  $SO_3^-$  from 80% to 95% relative humidity. Depending on the thermal history of Nafion, its water content can reach  $\sim 24$  mol  $H_2O$ /mol  $SO_3^-$  when equilibrated in liquid water or saturated water vapor.<sup>26</sup>

Three-dimensional renderings of images were made using Asylum's ARgyle Light software. Quantitative analysis of domain size and distribution was done using Asylum's MFP-3D software

in Igor Pro. Hydrophilic domains were defined by applying a threshold to a phase image such that points below the threshold marked the domains. Thresholds were readily chosen for attractive mode images, which have clearly defined domains. For these images, approximately the same threshold was arrived at using the iterative method,<sup>27</sup> the method of maximizing the number of domains as described by James et al.,<sup>28</sup> and by inspection of domain boundaries in line cuts and 2-D representations of a phase image. For repulsive mode images, however, domain boundaries were less distinct and only inspection of line cuts and 2-D representations of phase images proved to be a consistent method for determining the appropriate threshold. For consistency, this approach was used to determine domain boundaries in both attractive and repulsive mode images. In order to account for the size of the probe, domains smaller than  $20 \text{ nm}^2$  were excluded from analysis. Scan parameters were used to control whether imaging in attractive or repulsive mode. Attractive tip-sample interactions are favored for low oscillation amplitudes ( $\sim 10$  nm), amplitude set points near the free space amplitude ( $A/A_0 \approx 85\text{--}90\%$ ), cantilevers with high quality factors, and drive frequencies above resonance.<sup>21,29</sup> For repulsive mode imaging, drive frequencies were offset on the low frequency side of  $\omega_0$  at values corresponding to amplitudes 2–5% less than the amplitude at  $\omega_0$ . For attractive mode imaging, the offset was 2%, on either the low or high frequency side of resonance. Offsets in the drive frequency are illustrated in the Supporting Information (Figure S1). Different combinations of the above scan parameters facilitated attractive mode imaging. For example, both large oscillation amplitudes ( $\sim 50$  nm) with set point ratios of  $\sim 90\%$  and low oscillation amplitudes ( $\sim 20$  nm) with set point ratios of  $\sim 75\%$  yielded similar attractive mode phase images of Nafion. Our experience, however, is that a much smaller window of parameters exists for images taken in attractive mode than in repulsive mode. Real time monitoring of phase values allowed us to determine if the tip was experiencing net positive or net negative forces, as did histograms of the phase values in a given image. Scan speeds for both attractive and repulsive mode imaging ranged from 0.5 to  $2.5 \mu\text{m/s}$ .

## RESULTS AND DISCUSSION

For attractive and repulsive mode phase images taken on the same area of a Nafion membrane, aqueous surface domains are more spatially resolved in attractive mode (Figure 1). In the attractive mode image, areas of dark contrast (those closer to  $90^\circ$ ) correspond to greater power dissipations relative to areas of bright contrast, and are thus assigned to hydrophilic domains, as more damping is expected to be associated with the increased water content that accompanies such domains. This assignment agrees with the morphology of proton conducting domains observed in TEM images of stained Nafion.<sup>30–33</sup> Particle analysis reveals the average hydrophilic domain in the attractive mode image covers  $88 \text{ nm}^2$ , corresponding to an 11 nm diameter for circular domains, which is  $\sim 5$  nm larger than that observed in TEM images of Nafion stained with heavy cations,<sup>30,32</sup> but in agreement with those of Nafion stained with solid metal particles.<sup>33,34</sup> Being that TEM imaging is performed under vacuum and that AFM imaging in this work was done at ambient conditions, it is expected that membranes stained with solid metal particles would better reflect the pore structure of Nafion hydrated at ambient conditions than a membrane stained with metal cations.

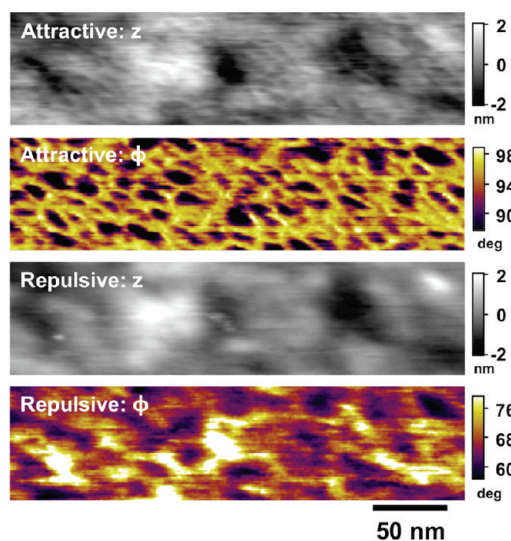


**Figure 1.** Height ( $z$ ) and corresponding phase images ( $\phi$ ) taken in attractive and repulsive modes on the same area of a Nafion membrane at ambient conditions (63% relative humidity). Image size:  $300 \times 75$  nm.

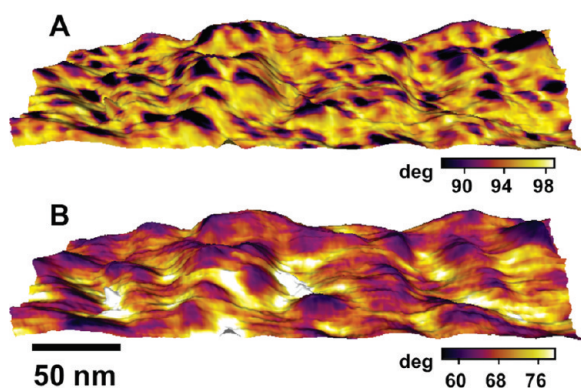


**Figure 2.** (A) Attractive and (B) repulsive mode phase contrast from Figure 1 colored onto 3-D representations of the repulsive mode topography.

Despite noticeable differences in resolution, areas of dark contrast in the repulsive mode phase image in Figure 1 correlate with areas of dark contrast in the attractive mode image, suggesting hydrophilic domains also contribute to phase contrast under net repulsive tip–sample interactions. However, where hydrophilic domains correspond to larger power dissipations in attractive mode, they correspond to lower dissipations in repulsive mode (phase farther from  $90^\circ$ ), indicating different sources of dissipation exist in the two modes. Overlaying the attractive and repulsive mode phase images onto a 3-D representation of the repulsive mode topography (Figure 2) reveals that phase contrast in attractive mode is independent of topography while phase contrast in repulsive mode is influenced by topography. In the repulsive mode phase image, areas with the largest power dissipation (bright contrast) often correlate with low-lying features in the topography. Such topographic valleys allow a larger portion of the tip's cone-like geometry to interact with the surface, resulting in larger power dissipations relative to other areas. Thus, topography represents an additional source of dissipation in repulsive mode. The attractive mode overlay in Figure 2 reveals that hydrophilic domains are associated with

both tall and low-lying height features, suggesting fluorocarbon and sulfonic acid functional groups in Nafion do not preferentially arrange according to topographic features as previously suggested.<sup>3</sup> Quantitatively, 50.1% of hydrophilic domains in the attractive mode phase image in Figure 1 are associated with topographic features at heights greater than the average height (by convention, 0 nm), which describes an even distribution of hydrophilic domains among tall and low lying features. However, for the repulsive mode image over the same area, 62.1% of hydrophilic domains are found at topographic features above the average height, which is due to the coupling of phase contrast and topography in this mode. We observe similar distributions of hydrophilic domains with regard to topography in other sets of attractive and repulsive mode images but should point out that the degree of topographic coupling varies with scan parameters.

Furthermore, hydrophilic domains in the attractive mode phase image in Figure 1 cover 25% of the surface (in 2-D), a value that agrees with our analysis of published TEM images, where we found domain coverages of 21%<sup>34</sup> and 28%.<sup>33</sup> For the repulsive mode image, areas one would assign as hydrophilic (i.e., dark contrast) cover 35% of the image's area, which is 1.4 times greater than in attractive mode. Not only does the repulsive mode image indicate a greater coverage by hydrophilic domains but also the individual domains are substantially larger. Particle analysis reveals the average hydrophilic domain in repulsive mode covers  $350 \text{ nm}^2$ , approximately four times the area of those measured in attractive mode ( $88 \text{ nm}^2$ ) and twice the diameter for circular domains (21 nm vs 11 nm). Incongruities in the two imaging regimes are also quantified by the number of domains in each image,  $2.7 \times 10^{-3}$  domains/ $\text{nm}^2$  in attractive mode and  $0.9 \times 10^{-3}$  domains/ $\text{nm}^2$  in repulsive mode. The higher resolution of phase contrast in attractive mode is attributed to the lower tip–sample interaction forces experienced in this regime, a result also observed in biological samples.<sup>35</sup> Masks used to calculate domain coverage, size, and occurrence are shown in Figure S2.

It should be noted that despite differences in resolution of phase contrast, the attractive and repulsive mode height images have similarly resolved features (Figure 1). Long range attractive forces often dominate tip–sample interactions in attractive mode, and for stiff surfaces (i.e., Si, mica, etc.), the probe does not make contact with the surface, instead oscillating a few nanometers above it.<sup>21</sup> However, for compliant substrates such as polyethylene, it has been shown that the tip can experience a net attractive force and make intermittent contact with the surface.<sup>21</sup> The small depressions seen in the attractive mode height image (Figure 1) are likely indicators of such jumps to contact. The attractive and repulsive mode images in Figure 1 were taken at a drive frequency with a  $-2\%$  offset and with a drive amplitude of  $\sim 25$  nm. Amplitude set point ratios of 80% and 60% were used for the attractive and repulsive mode images, respectively.

We have also found that contrast in repulsive mode phase images of Nafion membranes can arise from changes in topography (Figure 3), a result reported in phase imaging of biological samples.<sup>36</sup> Coupling of phase contrast with changes in topography becomes apparent when comparing images acquired over the same area of Nafion but taken in opposite scan directions. When scanning a sample at a 0 degree scan angle, the probe moves in the fast scan direction from left to right according to the scan size and then right to left over approximately the same area before significant motion occurs in the slow scan axis (top to bottom).

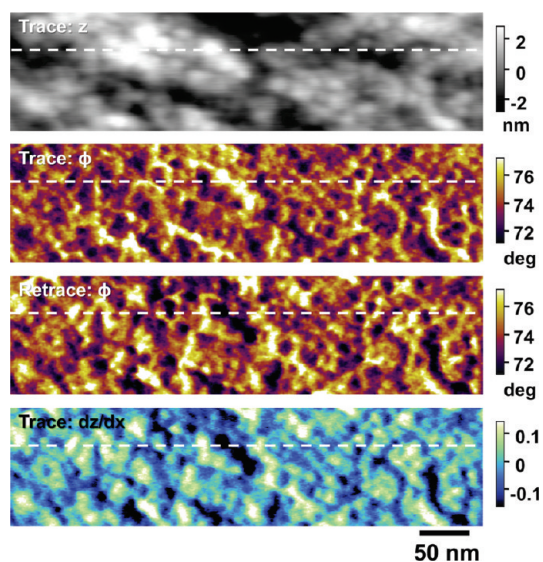


**Figure 3.** From top to bottom: height trace, phase trace, phase retrace, and derivative of the height trace with respect to  $x$  taken on a Nafion membrane at ambient conditions (34% relative humidity). Images taken in repulsive mode. Dashed lines indicate areas corresponding to the line profiles shown in Figure 4.

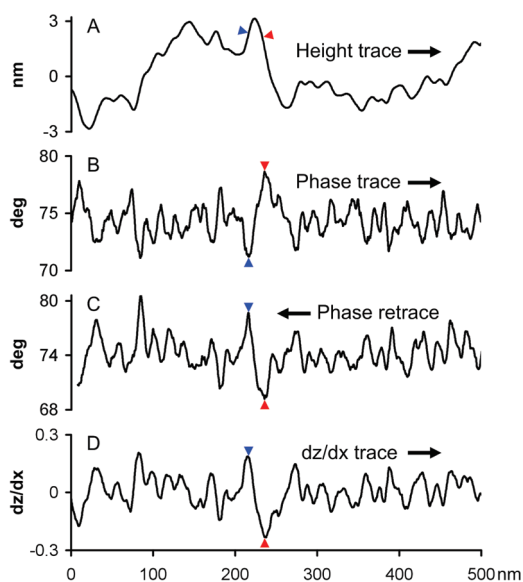


**Figure 4.** Line profiles from regions marked with dashed lines in Figure 3, (A) height trace, (B) phase trace, (C) phase retrace, and (D) derivative of the height trace. Arrows indicate scan direction, trace from left to right and retrace from right to left. As a guide, markers indicate valleys and peaks in the phase trace and retrace and the corresponding points in the height trace and in the derivative of the height trace.

A left to right scan direction is referred to as the “trace” while a right to left scan direction as the “retrace.”

Inspection of the phase trace and retrace images in Figure 3 reveals contrast is inverted in the two images. Furthermore, it appears that bright phase contrast in the trace image and dark phase contrast in the retrace image are related to tall height features. However, when comparing line profiles of the height image with those of the two phase images (Figure 4), we found that changes in topography are associated with peaks and valleys in

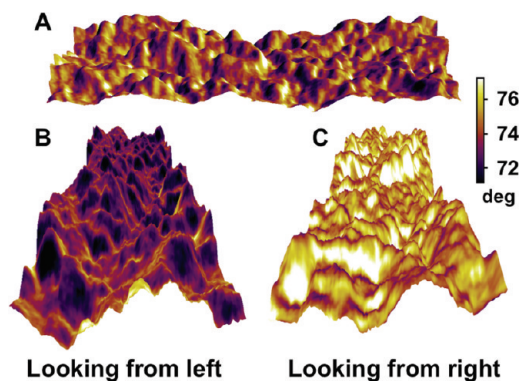


**Figure 5.** (A) phase trace image from Figure 3 colored onto a 3-D representation of the simultaneously acquired topography. Side views of (A) are shown in (B) and (C). Looking from the left corresponds to the probe climbing height features. Image size: 500 × 125 nm.

the phase images. The derivative of the height image (Figure 3) and a corresponding line profile from this image (Figure 4) reveal a pronounced correlation between changes in topography and phase contrast for the images in Figure 3. Specifically, dark phase contrast in the trace phase image is associated with positive changes in topography. That is, negative phase shifts occur as the probe ascends a height feature. If the probe climbs a height feature in the trace scan, it will descend that same feature in the retrace. Thus, for cases when phase contrast is coupled to changes in topography, contrast will be inverted for the two scan directions as seen in Figure 3. The magnitude of coupling between changes in topography and phase contrast is dramatically illustrated when contrast from the phase trace is colored onto a 3-D rendering of the height trace (Figure 5). Viewing this representation from the left (Figure 5A) shows the association of negative phase shifts with ascents of height features and viewing from the right shows the association of positive phase shifts with descents of height features (Figure 5B). A similar phenomenon was observed when the phase retrace was overlaid on the corresponding topography (Figure S3). The height and phase images in Figure 3 were acquired at a drive frequency with a  $-5\%$  offset, with a drive amplitude of  $\sim 50$  nm, and with an amplitude set point ratio of 75%.

While phase shifts can arise from changes in topography, this is not the case for all phase images. The contrast in both the attractive and repulsive mode phase images in Figure 1 show no dependence on changes in topography or scan direction as illustrated in the derivatives of their height images (Figure S4) and side views of their phase overlaid on topography (Figures S5 and S6). Empirically, we have found that phase contrast is more likely to depend on changes in topography than differences in tip–sample interactions at aqueous and fluorocarbon domains when scan parameters (scan speed, gains, drive amplitude, drive frequency, and amplitude set point) are not optimized, as manifested in slight offsets between the trace and retrace line profiles in the  $x$  direction (fast scan direction). For Nafion, the length scale over which topography changes happens to be similar to the size of aqueous surface domains, making the origin of phase contrast not readily apparent without examining the relation between phase shifts and changes in topography. For example, in the retrace phase image in Figure 3 in which the phase contrast was related entirely to changes in topography, the average size of areas one would assign as hydrophilic domains (dark phase contrast) is  $270 \text{ nm}^2$ , which is similar to the domain

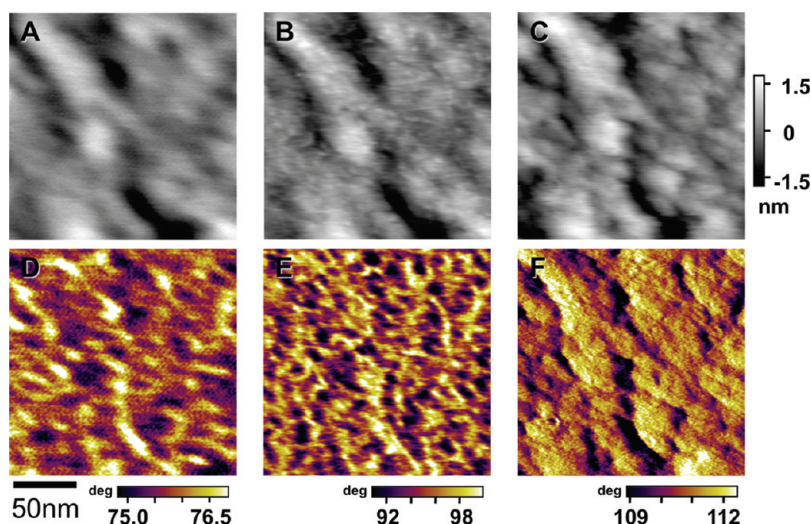


**Figure 6.** Height and corresponding phase images taken in (A) and (D) repulsive, (B) and (E) attractive, and (C) and (F) low power dissipation modes of the same area of a Nafion membrane at ambient conditions (relative humidity 32%). All images were taken in the trace scan direction. Image size:  $180 \times 180$  nm.

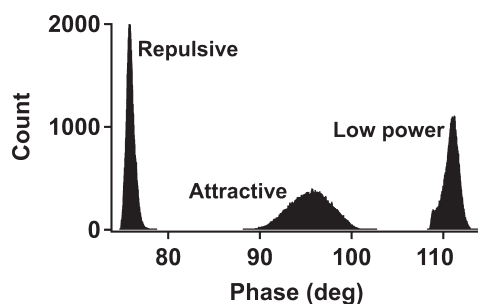


**Figure 7.** Distributions of phase values in the repulsive, attractive, and low power dissipation modes corresponding to Figure 6, panels D–F, respectively.

size observed in the repulsive mode phase image in Figure 1, where phase contrast was related to aqueous surface domains. Despite the resolution of features in the height and phase images in Figure 3, without decomposing into moments of topography,<sup>36</sup> phase contrast in the trace and retrace images cannot be assigned to hydrophilic and hydrophobic domains. Thus, in addition to tip–sample interaction regime, phase coupling to changes in topography must also be considered when interpreting phase images of PEMs.

We have also observed instances in which phase contrast in attractive mode is dominated by changes in topography. Figure 6 shows height and phase images corresponding to the same area of a Nafion membrane imaged in repulsive mode (Figure 6, panels A and D) and attractive mode (Figure 6, panels B, C, E, and F). Histograms showing the distributions of phase values in these three images are shown in Figure 7, where distributions below  $90^\circ$  correspond to net repulsive interactions, whereas those above  $90^\circ$  indicate net attractive interactions. In both Figures 6, panels E and F, the phase distributions are above  $90^\circ$ ; however, dramatic differences in morphology exist between these two attractive mode images. Figure 6E shows morphology, domain size, and domain distribution similar to the attractive mode image in Figure 1, yet Figure 6F shows phase contrast related only to the derivative of its height image (Figure S7). Instead of positive slopes in topography corresponding to negative phase shifts as in the repulsive mode images in Figure 3, the opposite is true for

Figure 6F; side views of phase contrast overlaid on topography illustrate how climbing a height feature is associated with positive phase shifts (Figure S8). As seen in the histograms in Figure 7, phase shifts in Figure 6F are closer to  $180^\circ$  than those in Figure 6E, which from the relationship between tip–sample power dissipation and the sine of the phase angle, indicates less power is dissipated in the former. Thus, we refer to the attractive mode phase image in Figure 6F as one with low power dissipation. We have found that driving the cantilever at frequencies above resonance typically results in low power dissipations. The repulsive mode images in Figure 6 were acquired at a drive frequency with a  $-5\%$  offset, with a drive amplitude of  $\sim 50$  nm, and with an amplitude set point ratio of 80%. Both sets of attractive mode images in Figure 6 were taken with a drive amplitude of  $\sim 20$  nm and amplitude set points of 75%; however, the low power images were taken with a  $+2\%$  offset in the drive frequency, whereas the attractive mode height and phase images in Figure 6, panels B and E, used a  $-2\%$  offset.

Within attractive mode, we have found a larger range of scan parameters facilitate low power dissipation images than the attractive mode images in Figures 1 and 6E. Thus, when interpreting phase images of PEMs taken in attractive mode, care must be taken to not mistake phase contrast related to changes in topography for contrast related to hydrophilic surface domains. The attractive and repulsive mode phase images in Figure 6, panels E and D, show average domain sizes and domain densities similar to those in Figure 1. The two data sets were taken several months apart and on different samples of Nafion 212 with different AFM probes. Attractive and repulsive mode images in Figure 6 have average hydrophilic domain sizes of 92 and 370  $\text{nm}^2$  and domain densities of  $2.6 \times 10^{-3}$  and  $0.9 \times 10^{-3}$  domains/ $\text{nm}^2$ , respectively. Masks used to calculate domain coverage, size, and occurrence are shown in Figure S9. The dramatic differences in phase contrast in Figure 6, panels D–F, taken over the same area of a Nafion membrane with the same probe testify to the importance of controlling tip–sample interactions. The subtle differences in the height images taken in repulsive, attractive, and low power modes also ascribe to the different nature of these modes. In particular, a larger portion of the tip contacts the surface in repulsive mode,

resulting in a height image (Figure 6A) that is less resolved than that in attractive (Figure 6B) and low power modes (Figure 6C). Furthermore, as in Figure 1, jumps to contact are visible in the attractive mode height image, yet do not exist in the low power mode height image, implying that the tip does not contact the sample in the latter.

## CONCLUSIONS

In this report, we have shown that interpretation of proton conducting domains mapped with AFM phase imaging strongly depends on whether net attractive or repulsive forces dominate tip-sample interactions. Specifically, the resolution of hydrophilic surface domains was maximized under net attractive forces. In fact, repulsive mode images taken of the same area of a Nafion membrane overestimate the size of hydrophilic surface domains by a factor of 4 ( $\sim 90 \text{ nm}^2$  vs  $\sim 360 \text{ nm}^2$ ) and underestimate the number of domains by a factor of 3 (2.7 domains per  $1000 \text{ nm}^2$  vs 0.9 domains per  $1000 \text{ nm}^2$ ). This has significant implications in describing the size, occurrence, and surface connectivity of proton conducting domains. Resolution in repulsive mode phase images was reduced as a result of coupling to topographic features. Also shown in this study were images taken in both repulsive and attractive modes whose phase contrast was related entirely to changes in topography. Without decoupling such effects,<sup>36</sup> phase contrast in these images is not meaningful in describing hydrophilic surface domains. While Nafion served as a model system in this study, differences in phase contrast for attractive and repulsive modes likely extend beyond Nafion to PEMs with similar chemical compositions<sup>37</sup> or morphologies.<sup>38,39</sup> The variation in phase contrast observed in this study for the same membrane illustrates the importance of controlling tip-sample interaction forces when using phase imaging to compare the nanoscale morphology of domains among membranes with different chemical structures and compositions. Finally, the size and occurrence of aqueous domains at the surface of Nafion membranes reported in this work represent values to which the properties of novel PEMs can be compared.

## ASSOCIATED CONTENT

**S** Supporting Information. Illustration of offsets in drive frequency. Masks used in particle analysis of phase images in Figure 1 and Figure 6. Side views of phase overlaid on topography corresponding to images in Figures 1, 3 (retrace), and 6 (low power). Derivatives of height images from Figures 1 and 6. This material is available free of charge via the Internet at <http://pubs.acs.org>.

## AUTHOR INFORMATION

### Corresponding Author

\*E-mail: buratto@chem.ucsb.edu. Tel: (805) 893-3393. Fax: (805) 893-4120.

## ACKNOWLEDGMENT

This work was supported by the MURI and DURIP programs of the U.S. Army Research Laboratory and U.S. Army Research Office under Grant Nos. DAAD 19-03-1-0121 and W911NF-09-1-0280. J.R.O. acknowledges the UCSB Graduate Student Science and Engineering Research Grant. This work utilized facilities in UCSB's Materials Research Laboratory, supported by

the MRSEC Program of the National Science Foundation under Grant No. DMR05-20415.

## REFERENCES

- (1) Hickner, M. A.; Ghassemi, H.; Kim, Y. S.; Einsla, B. R.; McGrath, J. E. *Chem. Rev.* **2004**, *104*, 4587–4611.
- (2) Tsang, E. M. W.; Zhang, Z.; Yang, A. C. C.; Shi, Z.; Peckham, T. J.; Narimani, R.; Frisken, B. J.; Holdcroft, S. *Macromolecules* **2009**, *42*, 9467–9480.
- (3) McLean, R. S.; Doyle, M.; Sauer, B. B. *Macromolecules* **2000**, *33*, 6541–6550.
- (4) James, P. J.; Antognozzi, M.; Tamayo, J.; McMaster, T. J.; Newton, J. M.; Miles, M. J. *Langmuir* **2001**, *17*, 349–360.
- (5) Wang, F.; Hickner, M.; Kim, Y. S.; Zawodzinski, T. A.; McGrath, J. E. *J. Membr. Sci.* **2002**, *197*, 231–242.
- (6) Gargas, D. J.; Bussian, D. A.; Buratto, S. K. *Nano Lett.* **2005**, *5*, 2184–2187.
- (7) Bussian, D. A.; O'Dea, J. R.; Metiu, H.; Buratto, S. K. *Nano Lett.* **2007**, *7*, 227–232.
- (8) Takimoto, N.; Wu, L.; Ohira, A.; Takeoka, Y.; Rikukawa, M. *Polymer* **2009**, *50*, 534–540.
- (9) Badami, A. S.; Lane, O.; Lee, H.-S.; Roy, A.; McGrath, J. E. *J. Membr. Sci.* **2009**, *333*, 1–11.
- (10) Lee, H. S.; Lane, O.; McGrath, J. E. *J. Power Sources* **2010**, *195*, 1772–1778.
- (11) Park, J. K.; Jones, P. J.; Sahagun, C.; Page, K. A.; Hussey, D. S.; Jacobson, D. L.; Morgan, S. E.; Moore, R. B. *Soft Matter* **2010**, *6*, 1444–1452.
- (12) Schmidt-Rohr, K.; Chen, Q. *Nat. Mater.* **2008**, *7*, 75–83.
- (13) Fan, F. F.; Bard, A. J. *Science* **1995**, *270*, 1849–1852.
- (14) Kang, Y. H.; Kwon, O.; Xie, X.; Zhu, D. M. *J. Phys. Chem. B* **2009**, *113*, 15040–15046.
- (15) Aleksandrova, E.; Hiesgen, R.; Friedrich, K. A.; Roduner, E. *Phys. Chem. Chem. Phys.* **2007**, *9*, 2735–2743.
- (16) O'Hayre, R.; Lee, M.; Prinz, F. B. *J. Appl. Phys.* **2004**, *95*, 8382–8392.
- (17) Chou, J.; McFarland, E. W.; Metiu, H. *J. Phys. Chem. B* **2005**, *109*, 3252–3256.
- (18) Kubo, W.; Yamauchi, K.; Kumagai, K.; Kumagai, M.; Ojima, K.; Yamada, K. *J. Phys. Chem. C* **2010**, *114*, 2370–2374.
- (19) Cleveland, J. P.; Anczykowski, B.; Schmid, A. E.; Elings, V. B. *Appl. Phys. Lett.* **1998**, *72*, 2613–2615.
- (20) Tamayo, J.; Garcia, R. *Appl. Phys. Lett.* **1998**, *73*, 2926–2928.
- (21) Garcia, R.; San Paulo, A. *Phys. Rev. B* **1999**, *60*, 4961.
- (22) Garcia, R.; Magerle, R.; Perez, R. *Nat. Mater.* **2007**, *6*, 405–411.
- (23) Mauritz, K. A.; Moore, R. B. *Chem. Rev.* **2004**, *104*, 4535–4585.
- (24) Kreuer, K. D.; Paddison, S. J.; Spohr, E.; Schuster, M. *Chem. Rev.* **2004**, *104*, 4637–4678.
- (25) Zawodzinski, T. A.; Neeman, M.; Sillerud, L. O.; Gottesfeld, S. *J. Phys. Chem.* **1991**, *95*, 6040–6044.
- (26) Onishi, L. M.; Prausnitz, J. M.; Newman, J. *J. Phys. Chem. B* **2007**, *111*, 10166–10173.
- (27) Ridler, T. W.; Calvard, S. *IEEE Trans. Syst., Man Cybernet.* **1978**, *8*, 630–632.
- (28) James, P. J.; McMaster, T. J.; Newton, J. M.; Miles, M. J. *Polymer* **2000**, *41*, 4223–4231.
- (29) Stark, R. W.; Schitter, G.; Stemmer, A. *Phys. Rev. B* **2003**, *68*, 085401.
- (30) Porat, Z.; Fryer, J. R.; Huxham, M.; Rubinstein, I. *J. Phys. Chem.* **1995**, *99*, 4667–4671.
- (31) Xue, T.; Trent, J. S.; Osseo-Asare, K. *J. Membr. Sci.* **1989**, *45*, 261–271.
- (32) Fujimura, M.; Hashimoto, T.; Kawai, H. *Macromolecules* **1982**, *15*, 136–144.
- (33) Rollins, H. W.; Lin, F.; Johnson, J.; Ma, J.-J.; Liu, J.-T.; Tu, M.-H.; DesMarteau, D. D.; Sun, Y.-P. *Langmuir* **2000**, *16*, 8031–8036.
- (34) Sun, Y.; Atornjitawat, P.; Lin, Y.; Liu, P.; Pathak, P.; Bandara, J.; Elgin, D.; Zhang, M. *J. Membr. Sci.* **2004**, *245*, 211–217.

- (35) San Paulo, A.; García, R. *Biophys. J.* **2000**, *78*, 1599–1605.
- (36) Stark, M.; Möller, C.; Müller, D. J.; Guckenberger, R. *Biophys. J.* **2001**, *80*, 3009–3018.
- (37) Ghielmi, A.; Vaccarone, P.; Troglia, C.; Arcella, V. *J. Power Sources* **2005**, *145*, 108–115.
- (38) Tsang, E. M. W.; Zhang, Z.; Shi, Z.; Soboleva, T.; Holdcroft, S. *J. Am. Chem. Soc.* **2007**, *129*, 15106–15107.
- (39) Yang, Y.; Shi, Z.; Holdcroft, S. *Macromolecules* **2004**, *37*, 1678–1681.